

Probing the behaviour of the X-ray binary Cygnus X-3 with very-long-baseline radio interferometry

V. Tudose,^{1,2,3,4*} J.C.A. Miller-Jones,^{5†} R.P. Fender,^{6,2} Z. Paragi,^{7,8} C. Sakari,⁹
A. Szostek,^{10,11} M.A. Garrett,¹ V. Dhawan,¹² A. Rushton,¹³ R.E. Spencer¹³
and M. van der Klis¹

¹*Netherlands Institute for Radio Astronomy, Postbus 2, 7990 AA Dwingeloo, the Netherlands*

²*Astronomical Institute ‘Anton Pannekoek’, University of Amsterdam, Kruislaan 403, 1098 SJ Amsterdam, the Netherlands*

³*Astronomical Institute of the Romanian Academy, Cutitul de Argint 5, RO-040557 Bucharest, Romania*

⁴*Research Center for Atomic Physics and Astrophysics, Atomistilor 405, RO-077125 Bucharest, Romania*

⁵*National Radio Astronomy Observatory, 520 Edgemont Road, VA 22903 Charlottesville, USA*

⁶*School of Physics and Astronomy, University of Southampton, Highfield, Southampton SO17 1BJ*

⁷*Joint Institute for VLBI in Europe, Postbus 2, 7990 AA Dwingeloo, the Netherlands*

⁸*MTA Research Group for Physical Geodesy and Geodynamics, P.O. Box 91, H-1521 Budapest, Hungary*

⁹*Whitman College, 345 Boyer Ave., WA 99362 Walla Walla, USA*

¹⁰*Laboratoire d’Astrophysique de Grenoble, UMR 5571 CNRS, Université Joseph Fourier, BP 53, 38041 Grenoble, France*

¹¹*Astronomical Observatory, Jagiellonian University, Orla 171, 30-244 Kraków, Poland*

¹²*National Radio Astronomy Observatory, 1003 Lopezville Road, NM 87801 Socorro, USA*

¹³*Jodrell Bank Centre for Astrophysics, School of Physics and Astronomy, University of Manchester, Manchester M13 9PL*

Accepted 2009 September 15. Received 2009 September 14; in original form 2009 July 16

ABSTRACT

In order to test the recently proposed classification of the radio/X-ray states of the X-ray binary Cyg X-3, we present an analysis of the radio data available for the system at much higher spatial resolutions than used for defining the states. The radio data set consists of archival Very Long Baseline Array data at 5 or 15 GHz and new electronic European Very Long Baseline Interferometry Network data at 5 GHz. We also present 5 GHz Multi-Element Radio Linked Interferometer Network observations of an outburst of Cyg X-3. In the X-ray regime we use quasi-simultaneous with radio, monitoring and pointed Rossi X-ray Timing Explorer observations. We find that when the radio emission from both jet and core is globally considered, the behaviour of Cyg X-3 at milliarcsecond scales is consistent with that described at arcsecond scales. However, when the radio emission is disentangled in a core component and a jet component the situation changes. It becomes clear that in active states the radio emission from the jet is dominating that from the core. This shows that in these states the overall radio flux cannot be used as a direct tracer of the accretion state.

Key words: accretion, accretion discs – stars: individual: Cygnus X-3 – ISM: jets and outflows – radiation mechanisms: non-thermal – techniques: interferometric.

1 INTRODUCTION

Cygnus X-3 (Cyg X-3) is an exotic X-ray binary system (XRB) discovered in the X-ray band by Giacconi et al. (1967). The nature of the compact object is unknown, circumstantial evidence existing for both a black hole (Cherepashchuk & Moffat 1994; Schmutz, Geballe & Schild 1996; Hjalmarsdotter et al. 2008; Szostek & Zdziarski 2008) and a neutron star (Tavani, Ruderman & Shaham

1989; Mitra 1998; Stark & Saia 2003). Strong evidence points toward a Wolf-Rayet star companion (van Kerkwijk et al. 1996; Fender, Hanson & Pooley 1999; Koch-Miramond et al. 2002) which makes Cyg X-3 a rather special object among the XRB population given the fact that at present only two other objects of this class, both extragalactic (Prestwich et al. 2007; Carpano et al. 2007), seem to harbour such a companion star type. The system is at a distance of 7–9 kpc (Predehl et al. 2000; Ling, Zhang & Tang 2009) and has an orbital period of 4.8 h inferred from infrared (e.g. Becklin et al. 1973) and X-ray (e.g. Parsignault et al. 1972) observations.

* E-mail: tudose@astron.nl (VT)

† Jansky Fellow, National Radio Astronomy Observatory

In the radio band the system shows flares of different amplitudes, the strongest of them reaching up to a few tens of Jy at cm wavelengths (e.g. Waltman et al. 1994; Trushkin, Nizhelskij & Bursov 2008). During these outbursts, Cyg X-3 reveals the presence of relativistic jets (Geldzahler et al. 1983; Spencer et al. 1986; Molnar, Reid & Grindlay 1988; Schalinski et al. 1995, 1998), with a complex structure that was clearly resolved in a few occasions (Mioduszewski et al. 2001; Martí, Paredes & Peracaula 2001; Miller-Jones et al. 2004; Tudose et al. 2007). Based on arcsec-scale radio observations Waltman et al. (1994, 1995, 1996) identified four distinct radio states of the system: quiescent (flux densities ~ 100 mJy), minor flaring (< 1 Jy), major flaring (> 1 Jy), and quenched (< 30 mJy).

In the X-ray band the study of Cyg X-3 has been hindered by the strong absorption existing in the system which is likely caused by the wind of the companion star (Szostek & Zdziarski 2008). The system shows two main X-ray states, hard and soft, plus a couple of transitional ones that are less understood (e.g. Hjalmarsdotter et al. 2009). These states are similar to the canonical X-ray states of black hole XRBs (e.g. Zdziarski & Gierliński 2004).

Quasi-simultaneous multi-wavelength studies, focused primarily on the X-ray and radio bands, have been carried out on Cyg X-3 (Watanabe et al. 1994; McCollough et al. 1999; Choudhury et al. 2002; Gallo, Fender & Pooley 2003; Szostek, Zdziarski & McCollough 2008). It was found that in quiescence the soft X-ray emission (< 12 keV) is correlated with the radio emission (GHz regime) and anti-correlated with the hard X-ray emission (> 20 keV). During major radio flares, the hard X-ray emission correlates with the radio emission, while the soft X-ray emission is anti-correlated with the radio emission. Recently, based on the relationship between the radio and soft X-ray emissions, Szostek et al. (2008) have revisited the classification of the radio states of Waltman et al. (1994, 1995, 1996), identifying six radio/X-ray states for Cyg X-3: quiescent, minor flaring, suppressed, quenched, major flaring, and post-flare.

2 OBSERVATIONS AND ANALYSIS

2.1 New e-VLBI data

Electronic very-long-baseline interferometry (e-VLBI) is a technique in which the data from radio telescopes separated by hundreds or thousands of km are streamed in real-time to the central data processor (i.e. the correlator). This technique is under continuous development and has been successfully used for the study of transient phenomena (Rushton et al. 2007; Tudose et al. 2007).

We observed Cyg X-3 with the European e-VLBI Network (e-EVN) at 5 GHz on five occasions, in 2007 Jun and 2008 Apr (Table 1). The data transfer rate was 256 Mbps for the run in 2007 and 512 Mbps for the rest. During the observations the target did not vary significantly in flux density with the exception of the run on 2007 Jun 25 when a smooth gradient was recorded during the first two hours. Although efforts were made to assure an accurate imaging of the data, artifacts might be present in the radio map for this epoch (Fig. 1). In particular, the reality of the extended

Table 1. e-EVN observations of Cyg X-3 at 5 GHz. The table contains the date of the observation, the corresponding modified Julian Day, the total observing time and the participating radio telescopes (Cm-Cambridge, Mc-Medicina, Jb2-Jodrell Bank Mk2, On-Onsala, Tr-Torun, Wb-Westerbork).

Date	MJD day	Total time h	Radio telescopes
2007 Jun 25	54276	10.3	Cm Mc Jb2 On Tr Wb
2008 Apr 09	54565	8.0	Cm Mc Jb2 On Tr Wb
2008 Apr 23	54579	10.3	Mc Jb2 Tr Wb
2008 Apr 25	54581	10.0	Cm Mc Jb2 Tr Wb
2008 Apr 27	54583	9.1	Cm Mc Jb2 Tr Wb

radio emission towards South-West is hard to assess with certainty. It appears also in the image made with a segment of the whole data set, when no variations in the amplitude took place and therefore it seems not to be an artifact.

The data were calibrated in AIPS (e.g. Greisen 2003) and imaged in DIFMAP (Shepherd 1997) using standard procedures. We used, upon availability, 3C 345 or 3C 84 as a fringe finder. J2007+4029, located 4.7° away from Cyg X-3 was the phase referencing calibrator. To improve on the amplitude calibration of the data we used the unresolved calibrator J2002+4725. Corrections of the antenna gains have been applied manually by imposing explicitly a constraint on the flux density of the mentioned point-like source, more exactly 0.5 Jy, as implied by the data.

2.2 Archival VLBA and previous e-VLBI data

In order to maximize the size of the sample to be used in the study we complemented the recent e-VLBI observations with archival Very Long Baseline Array (VLBA) and previous e-VLBI data. Whenever 5 GHz data were not available, we used 15 GHz observations. This choice was motivated by the fact that this was the frequency closest to 5 GHz for which a relatively large amount of data was present in the archive. Whenever possible we used the results published in the literature (see the column “comments” in Table 2), however, some data have not been reported before or the information of interest to us (e.g. flux densities) was not available and in these cases we calibrated and imaged the data using standard procedures (see references in section 2.1). Before imaging, a selection in the uv -plane was made for the VLBA data, the details and reasons of which are presented in section 2.3. The calibrators 3C 84 or J2202+4216 were used as fringe finders. Phase referencing was performed involving J2052+3635 or J2025+3343, situated respectively 5.9° and 7.4° away from Cyg X-3. For four epochs, not listed in Table 2, three from 2000 Apr and one from 1995 May, it was not possible to identify with certainty the location of the target and hence were not considered in the study.

2.3 MERLIN data

In support to the VLBI observations we also used Multi-Element Radio Linked Interferometer Network (MERLIN)

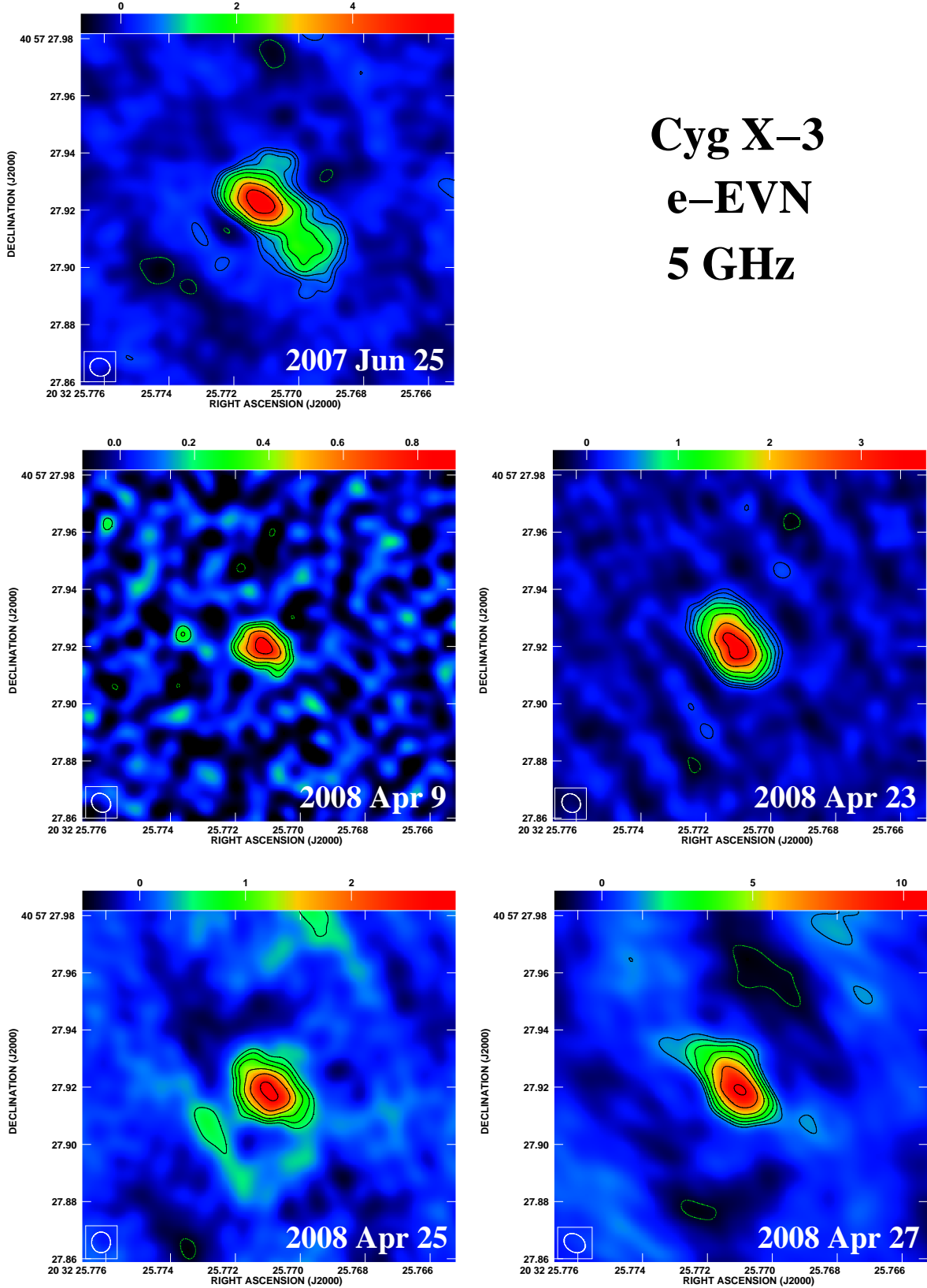


Figure 1. 5 GHz e-EVN radio maps of Cyg X-3. The contours are at the levels of -2.8, 2.8, 4, 5.6, 8, 11, 16, 23, 32, 45, 64, 90 times the rms noises of respectively 0.15, 0.07, 0.10, 0.17 and 0.45 mJy beam⁻¹. The grey code bars on top of the maps are expressed in mJy beam⁻¹.

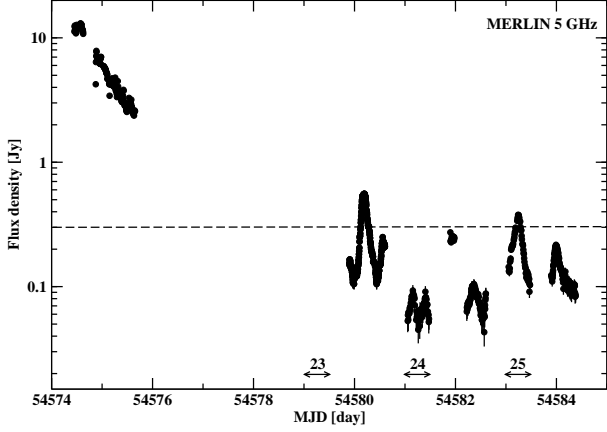


Figure 2. 5 GHz MERLIN 5 min averaged radio light curve of Cyg X-3 between 2008 Apr 18-Apr 28. The time intervals of the e-EVN observations and their number (see Table 2) are indicated. The horizontal dashed line corresponds to the transition level of 300 mJy (see section 3).

data for the Cyg X-3 outburst of 2008 April (Fig. 2). MERLIN was operated for approximately 80 h between April 18–April 28 at 5 GHz with 6 radio telescopes: Jodrell Bank Mk2, Cambridge, Knockin, Darnhall, Pickmere and Defford. The resulting maximum baseline length was 217 km, i.e. about 3.5 Mλ at 5 GHz. The flux density scale was determined from observations of 3C 286, using the three short baselines between the Jodrell Bank Mk2, Pickmere and Darnhall radio telescopes. A flux density of 7.361 Jy was assumed for 3C 286 (Perley et al. 1986). We used J2007+4029 as phase-referencing calibrator.

Only a small part of the flux density detected by MERLIN is recovered at the VLBI scales. This is due to the lack of relatively short baselines in the EVN array.

2.4 Analysis of radio VLBI data

Cyg X-3 is heavily scattered (Wilkinson et al. 1994) and this is of relevance for VLBI observations. The size of the scattering disc is (Mioduszewski et al. 2001):

$$\theta = 448 \left(\frac{\nu}{\text{GHz}} \right)^{-2.09} \text{ mas} \quad (1)$$

meaning about 15 mas at 5 GHz and 1.5 mas at 15 GHz.

The maximum uv -distance for which the data contain useful information is then given by:

$$uv_{\text{max}} = \frac{206.265}{448} \left(\frac{\nu}{\text{GHz}} \right)^{2.09} \text{ M}\lambda \quad (2)$$

corresponding to 13 Mλ at 5 GHz and 132 Mλ at 15 GHz.

All the e-EVN observations reported here and labeled as such in column “comments” of Table 2 were observed at 5 GHz. Their maximum intrinsic uv -distance is about 24 Mλ. A cut at 13 Mλ was found to be unnecessary with respect to

improving the image quality and so the values given in Table 2 are based on maps with the original uv -distance range.

For the VLBA data the situation is different. Their maximum nominal uv -distance is around 140 Mλ at 5 GHz and close to 440 Mλ at 15 GHz. Imposing an upper cut in the uv -distance plane according to the limits given by equation (2) did result in a significant increase in the quality of the maps. We therefore adopted the procedure for all the VLBA data sets we analyzed. The only exceptions are the epochs from 2001 Sep when we quote the results from Miller-Jones et al. (2004). This is justified by the fact that these authors limit the maximum uv -distance taken into account in the imaging process by selecting a group of close-by antennae, which it turned out produced a very similar effect on the uv -plane to what our approach would. The two methods rendered insignificant differences in the resulting radio maps.

The total flux densities (of core plus jets, if present) were measured in the image-plane using DIFMAP or AIPS. uv -plane fitting with elliptical Gaussians were also performed under DIFMAP as a check and the results were consistent, within the errors.

The core flux densities are less secured, despite the quoted errors, due to unknown systematics. One of the largest source of uncertainty is the lack of knowledge of the precise proper motion of Cyg X-3. In this paper we adopt the value of the proper motion obtained by analyzing the VLBI data listed in Table 2. The detailed results are presented elsewhere (Miller-Jones et al. 2009b).

In order to obtain the core flux density, whenever a jet was present in the image we subtracted it in the uv -plane and then measured the flux density at the expected position of the core after correcting for the proper motion. This approach is sensitive to any errors associated with the phase referencing process. Given the fact that for the VLBA observations the distance between the target and the phase reference calibrators was significant, such errors cannot be ruled out. In fact, in a few cases (flagged with a minus sign in the fourth column of Table 2) it was impossible to identify the core because of evident shifts from the expected position of Cyg X-3 which likely were due to unsuccessful phase referencing. However, in many of the images the target actually appeared as a single compact emitting region and we assumed it to be the core of the system, irrespective to any small shifts from the expected position as registered in a minority of cases.

Correctly locating the core has far reaching consequences. Building their argument on the apparent lack of proper motion of what was considered to be the core in VLBA data separated by 4.5 yr (Mioduszewski et al. 2001; Miller-Jones et al. 2004), Tudose et al. (2007) suggested that one of the compact emitting regions (denoted “knot C”) in their e-EVN data (from 2006 May 18) is probably not the core of the system. However, in the light of the new knowledge provided by the analysis of the VLBI data with respect to the proper motion of the system, it is almost sure that “knot C” is actually the core. This has important implications with respect to the orientation of the jet of Cyg X-3, but are beyond the scope of this work and are addressed elsewhere (Miller-Jones et al. 2009b). The core flux density reported in Table 2 for the 2006 May 18 epoch is the flux density of “knot C”.

Table 2. Observational log. The table contains the number of the observation, the corresponding date, the frequency of the radio observation, the radio flux densities of the core and core+jet, the ASM-RXTE count rate in the 3–5 keV energy band, the hardness ratio $HR2=(5\text{--}12\text{ keV})/(3\text{--}5\text{ keV})$, and comments.

Obs nr.	Date	Freq. GHz	Core FD mJy	Total FD mJy	CR (ASM) c s^{-1}	HR2	Comments
1	1997 Feb 06 (MJD 50485)	15	224 ± 10	1800 ± 200	6.48 ± 0.09	1.59 ± 0.03	
2	1997 Feb 08 (MJD 50487)	15	167 ± 5	537 ± 50	6.59 ± 0.10	1.50 ± 0.03	
3	1997 Feb 11 (MJD 50490)	15	611 ± 5	611 ± 5	7.58 ± 0.10	1.41 ± 0.02	
4	2000 Apr 02 (MJD 51636)	5	1500 ± 15	1500 ± 15	10.45 ± 0.33	1.09 ± 0.05	
5	2000 Apr 03 (MJD 51637)	5	870 ± 6	870 ± 6	12.08 ± 0.31	1.17 ± 0.04	
6	2000 Apr 21 (MJD 51655)	5	-	1890 ± 262	5.86 ± 0.13	1.86 ± 0.05	
7	2001 Sep 18 (MJD 52170)	5	21 ± 5	13120 ± 300	6.96 ± 0.18	1.68 ± 0.06	Miller-Jones et al. (2004)
8	2001 Sep 19 (MJD 52171)	5	-	13120 ± 300	6.23 ± 0.13	1.89 ± 0.05	Miller-Jones et al. (2004)
9	2001 Sep 20 (MJD 52172)	5	-	6120 ± 300	5.11 ± 0.11	1.97 ± 0.05	Miller-Jones et al. (2004)
10	2001 Sep 21 (MJD 52173)	5	39 ± 5	4736 ± 300	6.22 ± 0.14	1.85 ± 0.05	Miller-Jones et al. (2004)
11	2001 Sep 22 (MJD 52174)	5	73 ± 5	2922 ± 300	4.96 ± 0.20	2.20 ± 0.10	Miller-Jones et al. (2004)
12	2001 Sep 23 (MJD 52175)	5	8 ± 2	1389 ± 300	6.34 ± 0.12	1.74 ± 0.04	Miller-Jones et al. (2004)
13	2002 Feb 15 (MJD 52320)	15	77 ± 6	77 ± 6	9.88 ± 0.26	1.00 ± 0.04	
14	2004 Jan 11 (MJD 53015)	15	136 ± 4	136 ± 4	1.74 ± 0.16	2.65 ± 0.27	ASM data from 2004 Jan 3
15	2004 Oct 17 (MJD 53295)	15	98 ± 3	98 ± 3	1.68 ± 0.09	2.29 ± 0.15	
16	2004 Nov 21 (MJD 53330)	15	59 ± 2	59 ± 2	1.29 ± 0.09	3.10 ± 0.25	
17	2005 Jun 10 (MJD 53531)	15	65 ± 1	65 ± 1	1.29 ± 0.12	2.56 ± 0.28	ASM data from 2005 Jun 17
18	2005 Dec 28 (MJD 53732)	15	63 ± 2	63 ± 2	3.52 ± 0.34	2.04 ± 0.23	
19	2006 Apr 20 (MJD 53845)	5	87 ± 9	87 ± 9	6.92 ± 0.15	1.40 ± 0.05	e-EVN; Tudose et al. (2007)
20	2006 May 18 (MJD 53873)	5	101 ± 3	909 ± 18	5.79 ± 0.11	1.70 ± 0.04	e-EVN; Tudose et al. (2007)
21	2007 Jun 25 (MJD 54276)	5	23 ± 1	42 ± 3	2.40 ± 0.12	2.24 ± 0.13	e-EVN
22	2008 Apr 09 (MJD 54565)	5	4 ± 1	4 ± 1	8.91 ± 0.15	1.14 ± 0.03	e-EVN
23	2008 Apr 23 (MJD 54579)	5	52 ± 4	52 ± 4	7.27 ± 0.45	1.65 ± 0.17	e-EVN
24	2008 Apr 25 (MJD 54581)	5	19 ± 1	19 ± 1	10.83 ± 0.21	1.25 ± 0.04	e-EVN
25	2008 Apr 27 (MJD 54583)	5	62 ± 1	62 ± 1	7.77 ± 0.14	1.31 ± 0.04	e-EVN

A clarification has to be made as well with respect to the short communication presented by Tudose et al. (2008) about the e-EVN run on 2008 Apr 9. The authors report that the preliminary analysis of the data reveals the presence in the radio map of two distinct compact emitting regions. After a detailed analysis we discovered that one of those emitting regions is an artifact. This was due to a temporary bug in the standard post-correlation software used prior to the data release, which allowed for visibilities near scan boundaries to appear in both scans, thus resulting in phase-reference source visibilities in the Cyg X-3 data. This way an artificial source was introduced near the phase-centre. Coincidentally, the location of the artifact was very close to the position of a compact emitting region (“knot A”) observed in the e-EVN observations of 2006 May 18 making it even more believable. In Fig. 1 we present the correct version of the radio map corresponding to the 2008 Apr 9 epoch.

Note that the term “core” used throughout the paper does not necessarily reflect the actual size of Cyg X-3 system (i.e. the size of the region at whose boundaries the optical depth for the radio emission becomes unity). Miller-Jones et al. (2009a) used the minimum variability timescales observed during a period of low-level activity to set constraints on the size of the source at 43 GHz and 15 GHz. For an outflow traveling at the speed of light at a distance of 10 kpc it translated in a size of 0.2–0.3 mas. This is smaller than the size of the scattering disc at the two frequencies we used here.

2.5 X-ray data

We used Rossi X-ray Timing Explorer (RXTE) All Sky Monitor (ASM)/Proportional Counter Array (PCA)/High-Energy X-ray Transient Experiment (HEXTE) data observed quasi-simultaneously (i.e. within one day) with the radio observations.

As pointed out for instance by Szostek et al. (2008), due to the shape of the X-ray spectra the best ASM band to study the radio/X-ray correlation in Cyg X-3 is the 3–5 keV and therefore further on, unless otherwise noted, we will refer to this band whenever an ASM count rate is quoted. To calculate the hardness ratio (HR2) we used the ASM count rates in the 5–12 keV and 3–5 keV bands. In order to put the particular values used in this work in retrospective, Fig. 3 shows the variations of the ASM count rate and hardness ratio between 1996 Nov–2008 May.

In the case of PCA we used the first layer only and the Proportional Counter Units (PCU) 0 and 2, or 1 and 2, upon availability. For HEXTE we analyzed data from either clusters A or B. The X-ray spectra were extracted in the PCA energy band 3–20 keV and HEXTE energy band 15–90 keV. The spectra were fitted in XSPEC11 (e.g. Arnaud 1996) with a model including Comptonization by thermal and non-thermal electrons (EQPAIR; Coppi 1992, 1999; Gierliński et al. 1999), Compton reflection (PEXRIV; Magdziarz & Zdziarski 1995), absorption by two neutral media, fully and partially covering the source (ABSND), and a broad Gaussian Fe $K\alpha$ fluorescent line (GAUSS). Sim-

Table 3. Classification of the PCA/HEXTE-RXTE X-ray spectra of Cyg X-3. The spectra were taken quasi-simultaneously with the radio data in Table 2. The table lists the number of the observation (associated to first column of Table 2), the date, the RXTE ID of the observation, the detectors used, and the X-ray spectral group following the nomenclature of Szostek et al. 2008.

Obs nr.	Date	Obs ID	Detectors	Spectral group
5	2000 Apr 03 (MJD 51637)	50062-02-01-00	PCU 0,2; HEXTE A	5
6-1	2000 Apr 22 (MJD 51656)	50062-01-01-00	PCU 0,2; HEXTE A	4
6-2	2000 Apr 22 (MJD 51656)	50062-01-01-01	PCU 0,2; HEXTE A	3
20-1	2006 May 17 (MJD 53872)	91090-03-01-00	PCU 0,2; HEXTE B	3/4 ?
20-2	2006 May 17 (MJD 53872)	91090-03-02-00	PCU 0,2; HEXTE B	3/4 ?
23	2008 Apr 23 (MJD 54579)	93434-01-01-00	PCU 1,2; HEXTE B	3/4 ?
24	2008 Apr 25 (MJD 54581)	93434-01-02-00	PCU 1,2; HEXTE B	5
25	2008 Apr 27 (MJD 54583)	93434-01-03-00	PCU 1,2; HEXTE B	4

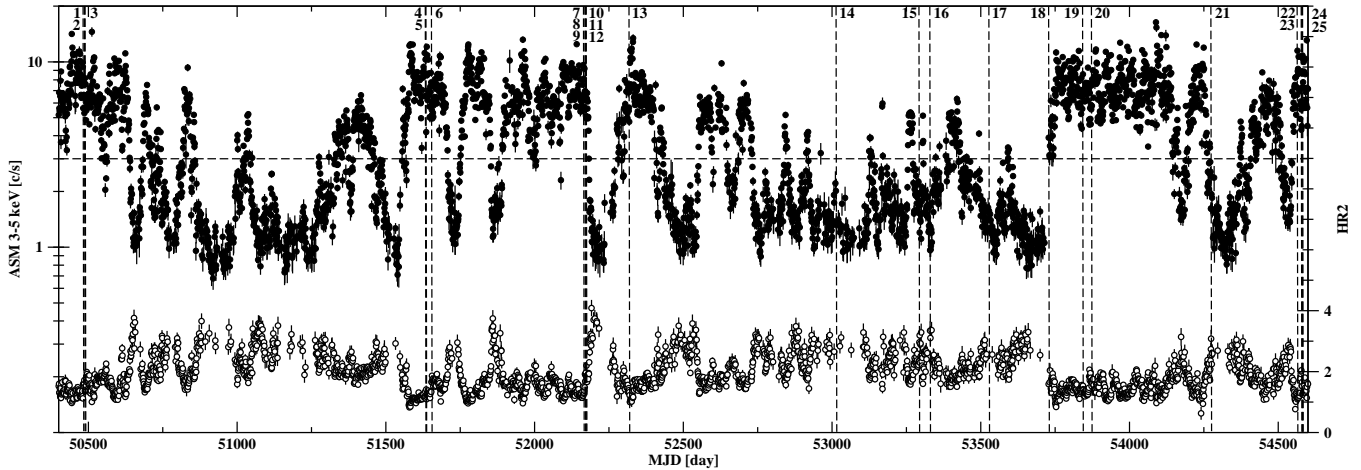


Figure 3. The daily-averaged ASM-RXTE 3–5 keV light curve of Cyg X-3 between 1996 Nov–2008 May (filled circles) and the ASM-RXTE hardness ratio $HR2 = (5–12 \text{ keV}) / (3–5 \text{ keV})$ for the same object and time interval (empty circles). The vertical dashed lines correspond to the radio observations in Table 2, labeled by observation number. The horizontal dashed line corresponds to the transition level of 3 counts s^{-1} (see section 3).

ilar models were used for Cyg X-3 by Vilhu et al. (2003); Hjalmarsdotter et al. (2008); Szostek & Zdziarski (2008); Szostek et al. (2008). A detailed description of the model is given by Hjalmarsdotter et al. (2009). A systematic error of 3 per cent was added to the data. The fits had a reduced χ^2 around 1 or less.

Following Szostek et al. (2008) both in methodology and nomenclature (Fig. 4), the resulting absorbed spectra were classified according to their shape and flux at 20 keV (Table 3). In a few cases it was not possible to identify with certainty the X-ray spectral group.

3 MILLIARCSECOND BEHAVIOUR

Working with Green Bank Interferometer (GBI) radio data and ASM/PCA/HEXTE RXTE X-ray data between 1996–2000, Szostek et al. (2008) classified six radio/X-ray states of Cyg X-3. Four of them correspond to the radio states previously identified by Waltman et al. (1994, 1995, 1996)

using GBI observations obtained during the period 1988–1992. Fig. 5, upper panel (an adaptation of Figs. 4 and 6 of Szostek et al. 2008) shows the position of these states in a log-log representation of the radio versus X-ray flux, together with the corresponding X-ray spectral groups to which they can be associated. This schematic representation is purely phenomenological. It is based on the above cited works as well as on the VLBI data that will be discussed further on. The two transition levels, represented by the dashed lines, are chosen to coincide with the values favoured by Szostek et al. (2008): 3 counts s^{-1} ASM count rate and 300 mJy radio flux density at 8.3 GHz.

Based on the monitoring campaigns with GBI (e.g. Waltman et al. 1994), Ryle Telescope (e.g. Fender et al. 1997; Pooley 2006), RATAN-600 (e.g. Trushkin et al. 2006, 2008), strong evidence is mounting that major flares of Cyg X-3 are preceded by periods of quenched radio emission. Szostek et al. (2008) found that after a major flare state the system is entering the minor flaring or the suppressed states, via the post-flare stage. They also note that the minor flares happen during transitions, in both directions, between the

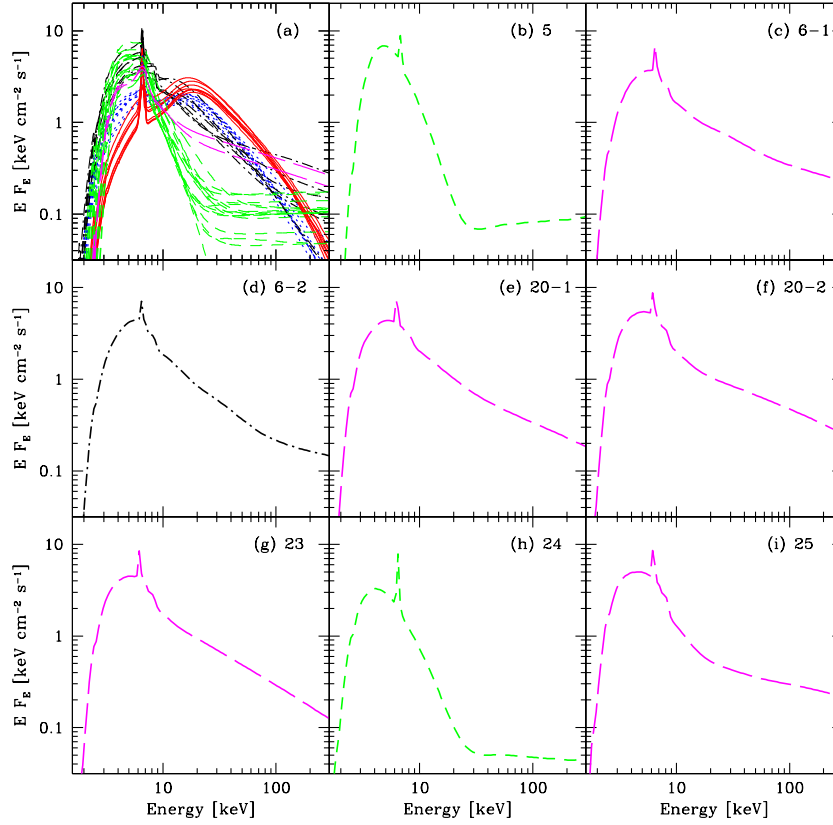


Figure 4. Classification of the X-ray spectra of Cyg X-3 (Szostek et al. 2008). *Panel a*): PCA/HEXTE-RXTE spectra of Cyg X-3 between 1996–2000. Group 1: continuous red line; Group 2: dotted blue line; Group 3: dash-dotted black line; Group 4: long-dashed magenta line; Group 5: short-dashed green line. *Panels b-i*): spectra corresponding to observations in Tabel 3. Numbers indicate the observation epoch. For representation purposes the spectra for epochs 20-1, 20-2 and 23 were considered to pertain to Group 4.

quiescence and the suppressed states. The changes through different states are mirrored by variations in the X-ray spectra. An approximate correspondence can be established between them (Szostek et al. 2008): spectral X-ray group 1 is associated to the quiescence state, group 2 to the minor flaring state, group 3 to the suppressed state, group 4 to the major flaring state, group 5 to the post-flaring state. This was a summary of a few of the characteristics of Cyg X-3 when the arcsec scale radio observations are considered. However, at VLBI scales (i.e. mas scales) extended radio emission (i.e. jets) was resolved (Mioduszewski et al. 2001; Miller-Jones et al. 2004; Tudose et al. 2007). Unfortunately, such high angular resolution radio observations are much more sparse than those at lower angular scales and hence it is not yet clear, for instance, what is the interplay between the radio emission from the core and from the jets, or what is the exact nature of the jets themselves (discrete knots of adiabatically expanding plasma or internal shocks propagating within a quasi-steady flow).

In this context, despite the limited amount of data available at the moment, an attempt at probing the behaviour of Cyg X-3 at mas scales has two important advantages over the arcsec scales approach: it potentially offers a more accurate image of the system, free of possible flux contamination

from other sources present in the field of view, and it gives the opportunity to disentangle the jet contribution to the total flux density.

Fig. 5, middle panel, shows the relation between the soft X-ray and radio emissions when both the contribution of the jet and core are taken into account in the radio band. In the same figure, in the bottom panel, the contribution of the jet to the radio flux density has been removed. As mentioned at the beginning of this section, the superimposed dashed lines should be taken as guides for the eye and reflect the model of the radio/X-ray states of Cyg X-3 as proposed by Szostek et al. (2008). In defining this scheme these authors used GBI data at 8.3 GHz, but noted that the use of 2.25 GHz GBI data or the 15 GHz Ryle Telescope data yielded relatively similar results. This gives us confidence that the use of the two frequencies in our study, namely 5 GHz and 15 GHz, on the one hand should not infringe on the direct comparison with their results, and on the other should not affect significantly any trend present in the data due to the unaccounted for effect of the shape of the radio spectrum at the moment of the observations. Regarding this latest aspect we also add that after the onset of an outburst period,

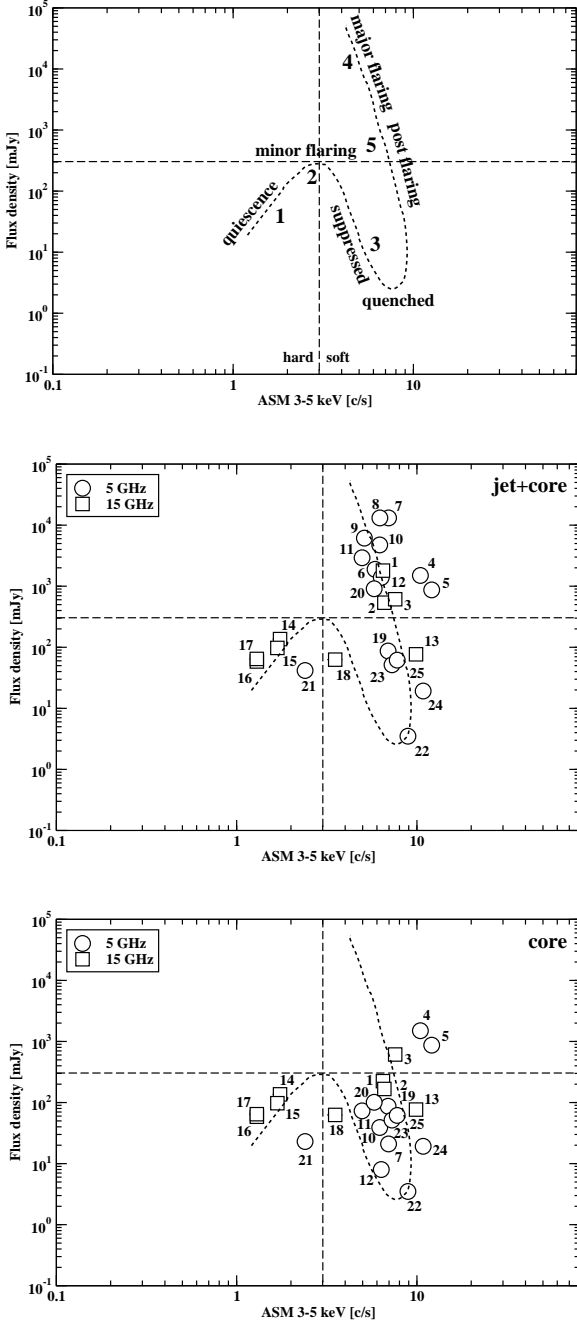


Figure 5. *Top:* The radio/X-ray states of Cyg X-3 as proposed by Szostek et al. 2008. The numbers correspond to the X-ray spectral group. The transition levels at 3 counts s^{-1} and 300 mJy are chosen to coincide with those used in the above cited reference. The curved dashed line is a guide for the eye and mirrors the trend found by those authors. *Middle:* Quasi-simultaneous radio/X-ray emission of Cyg X-3 when the radio emission of core and jet are both considered (data from Table 2). Radio data at 5 GHz represented with open circles and at 15 GHz with open squares. The numbers correspond to the observation number (first column of Table 2). *Bottom:* The same as middle panel, but this time only the radio emission from the core of the system is taken into account.

that is when the system is in the major flaring, post-flaring or minor flaring state, the radio spectrum between 5 and 15 GHz is usually optically thin (Miller-Jones et al. 2004; Trushkin et al. 2006; Lindfors et al. 2007; Trushkin et al. 2008; Miller-Jones et al. 2009a) which means that the 15 GHz flux densities from Table 2 and Fig. 5 corresponding to these three states are likely lower limits for the unknown 5 GHz flux densities. But again, given the log-log representation of Fig. 5, this should not affect any of the conclusions to follow.

With respect to Fig. 5, middle panel, acknowledging the small number of observations, the mas scale behaviour of Cyg X-3 does seem consistent with the arcsec scale one reported by Szostek et al. (2008) in their Figs. 4 and 5, at least from the point of view of the overall distribution of points and the normalization.

3.1 Quiescence state

The observations 14, 15, 16 and 17 strongly suggest that the system was in the quiescence state: the levels of the radio and X-ray emissions as well as the apparent correlation between them are those expected, but note that the X-ray data is not simultaneous with the radio on two of the epochs.

The observation 21 (2007 Jun 25) requires some discussion. About three weeks before, Cyg X-3 exhibited a major flare (Trushkin et al. 2007) with the peak flux density on 2007 Jun 1. Within one week the flux density decreased significantly, from ~ 3.5 Jy down to ~ 200 mJy and the monitoring stopped. No further indication with respect to the immediate radio evolution exists. However, one might make the case that during the observation 21 the system was likely in quiescence. It might be that after the major flare faded away, Cyg X-3 passing through the post-flare state entered the minor flaring state (via the suppressed state perhaps) and from there ended up in the quiescence. Then the jet observed on 2007 Jun 25 (Fig. 1), if real (see section 2.1), is the reminiscence of the excursion in the minor flaring state. Support for this scenario comes from the ASM X-ray data. After the major flare about 2007 Jun 1 the X-ray emission became harder, with count rates decreasing steadily from around 12 counts s^{-1} down to the transition level of 3 counts s^{-1} about 10 days later. The system crossed the threshold and after reaching 2 counts s^{-1} evolved back towards softer X-ray emission, crossed again the transition level and, finally, made a last pass over the 3 counts s^{-1} limit (close to 2007 Jun 20), ending up in the region of ~ 2 counts s^{-1} (and going dimmer) where it was probed by the radio observation of 2007 Jun 25.

3.2 Suppressed state

During the observation 18 Cyg X-3 was very likely in a suppressed state (see Fig. 4 of Trushkin et al. 2006). This state, introduced by Szostek et al. (2008), is characterized by the fact that it is not immediately followed by a major radio flare.

The isolated observation 13 on 2002 Feb 15 is quite hard to classify with certainty. The only independent radio information available is from the unpublished Ryle Telescope

data on G.G. Pooley's web page¹: the system was in a kind of suppressed state, just a few days before a quenched state.

3.3 Quenched state

On 2008 Apr 9 (observation 22; Fig. 1) Cyg X-3 was at the level of 4 mJy at 5 GHz. The system was in a quenched radio state. This is the faintest radio VLBI detection of Cyg X-3 at cm wavelengths so far. Two weeks later the system was already in an active state (observations 23, 24, 25). Such a behaviour is consistent with previous observations showing that major radio flares of Cyg X-3 are preceded by periods of quenched radio emission.

3.4 Major flare/post flare states

Two weeks after the faint radio detection on 2008 Apr 9, a series of three e-EVN observations (23, 24 and 25; Fig. 1), separated by 2 days followed. Meanwhile the system underwent a major outburst with the peak on 2008 Apr 18 (see Fig. 2) and these observations actually reveal Cyg X-3 during the descending stage of the flare (however, note the significant rebrightening on 2008 Apr 27). X-ray spectra were also available on these dates (Table 3). For observation 23 it is not clear to which group the spectrum belongs too; it might be group 3 or 4. Given the fact that the next two observations show spectra pertaining to groups 5 and 4 respectively, the likely interpretation is that the system didn't have time to reach the suppressed state by the time of observation 23, but was rather still in the major flaring/post-flaring states.

On 2006 Apr 20 and 2006 May 18 (observations 19 and 20; Fig. 2 of Tudose et al. 2007) Cyg X-3 was observed a few weeks and a few days respectively after the peak of two major flares. In the first instance the system was in a post-flare state, while in the second very likely still in the flare state. The X-ray spectrum taken on 2006 May 17 (Table 3) does not permit a clear classification, but given the radio data (e.g. the presence of a resolved jet) it would be perhaps reasonable to expect that the spectrum belongs to group 4.

The observations 1 to 3 started two days after a major flare and were made when the system was in the major flare/post-flare states (Fig. 1 of Mioduszewski et al. 2001). Much like during the e-EVN observations of 2008 Apr, a rebrightening event was detected on 1997 Feb 11, which can very likely be associated with the core of the system.

Some very interesting data were taken in 2000 Apr (observations 4, 5 and 6). No reference was found in the literature to these runs. According to unpublished Ryle Telescope data², the observations were made within a couple of days after two major outbursts. During observation 4 the system was in a major flare/post-flare state in which it persisted also during the observation 5, as suggested also by the X-ray spectrum (Table 3) with characteristics particular to group 5. Regarding observation 6, judging by the radio data alone, Cyg X-3 seemed to have been in a major flare/post-flare state. However, the X-ray data (Table 3) is intriguing since it suggests that the spectra changed during the run from

group 4 to group 3, i.e. the system switched from the flare state to the suppressed state. In the context of the model of Szostek et al. (2008), such an evolution is to be expected but not at this quite high radio flux density. Recalling the situation of the observation 20 for which the X-ray spectrum revealed ambiguity with respect to the exact classification we can note that in both cases, i.e. observations 6 and 20, the radio emission can be disentangled in a core component and a jet component (although for observation 6 it was impossible to identify with certainty the location of the core; see section 2.3). The high radio flux density in these cases is due to the jet component, while, perhaps, in fact the core of the system was already close to the suppressed state (see the location of observation 20 in Fig. 5, bottom panel, after removing the jet component). Anyway, this implies that very quick spectral changes are possible in the core of the system.

A very good coverage of the evolution of a major flare was obtained in 2001 Sep (observations 7–12; Fig. 1 of Miller-Jones et al. 2004). Cyg X-3 was observed at or slightly after the peak of the outburst and during the dimming phase. It is no doubt that these data correspond to the major flare state of the system.

3.5 Jet/core disentanglement

Insofar, the focus of the discussion was on the mas behaviour of Cyg X-3 when the radio emission from both the core and jet were taken into account. Removing this later component of the radio emission, we obtained the plot represented in Fig. 5, bottom panel. The trend in the distribution of the points observed at mas scale in Fig. 5 middle panel and which looks so similar to that observed at arcsec scales by Szostek et al. (2008) is lost. Basically what happens is that the data in Fig. 5 corresponding to the major flare/post-flare states, in which the jet emission is dominant, are shifted towards lower radio flux densities thus blurring the classification of the states, roughly speaking, beyond and below the ad-hoc X-ray and respectively radio transition levels. While these states may be able to be classified via their X-ray spectra, the radio emission cannot be used as a diagnostic here.

The important conclusion is that since in active states most of the radio emission is not coming from the core then during outbursts the overall radio flux is not a direct tracer of the accretion state.

However, when the overall radio flux is considered we do observe an anti-correlation/trend between the radio and X-ray emissions in the flare/post-flare states (Fig. 5, middle and Fig. 4 of Szostek et al. 2008). Moreover, also in the soft X-ray states of the system (more precisely on the major flare branch and part of the post-flare branch) Szostek et al. (2008) found a correlation/trend (their Fig. 7) between the radio emission and the hard X-rays in the energy band 20–100 keV as measured by the Burst and Transient Source Experiment (BATSE) on-board the Compton Gamma-Ray Observatory. These correlations or, more conservatively, trends are quite interesting and deserve an attempt at explanation. Using arcsec scale radio data Lindfors et al. (2007) and Miller-Jones et al. (2009a) fitted satisfactorily the light curves of Cyg X-3 during minor as well as major outbursts. They employed a shock-in-jet model originally developed by Marscher & Gear (1985) and later generalized by

¹ <http://www.mrao.cam.ac.uk/~guy/cx3/2002.ps.gz>

² <http://www.mrao.cam.ac.uk/~guy/cx3/2000.ps.gz>

Türler et al. (2000). The model assumes an adiabatically expanding, conical, constant Doppler factor jet through which a shock is propagating. Stronger radio flares seem to evolve on longer timescales than the fainter ones, consistent with the formation of the shocks downstream in the jet, further away from the core of the system. With this in mind, the radio/X-ray trends mentioned above can be qualitatively explained within the truncated disc model of the X-ray states (Remillard & McClintock 2006; Done, Gierliński & Kubota 2007 for reviews). In the soft X-ray states the innermost region of the accretion disk is relatively close to the compact object and slowly recedes further away as the outburst proceeds. As the disc gets colder the level of the soft X-rays (i.e. ASM and PCA energy bands) is decreasing, while the corona starts to build up leading to an increase in the hard X-rays (i.e. HEXTE and BATSE energy bands). Therefore stronger radio flares, which tend to peak at later times, will be associated with states in which the accretion disk is truncated further away from the compact object, where the soft X-ray levels are lower and the hard X-ray levels are higher. This explanation is reasonable, but it should be noted that other factors are likely to be involved in the behaviour of Cyg X-3 during major outbursts. For instance the interaction of the jet with the interstellar medium or the stellar wind from the companion is to be expected during major flares. The external shocks thus formed will perhaps contribute a fair amount of radio synchrotron radiation to the overall radio emission. Unfortunately the environment of Cyg X-3 is poorly known, and given also the orientation of the jets in the system, supposedly close to the line of sight, make any such estimations uncertain.

Continuing the discussion on the multi-wavelength behaviour, in some XRB systems in hard X-ray states correlations seem to exist between the radio and X-ray emissions. Also, above some X-ray flux, in the soft X-ray states, the radio emission drops significantly. These properties are relatively well established in the case of black hole XRBs (BHXRBS) [Corbel et al. 2003; Corbel, Körding & Kaaret 2008; Gallo, Fender & Pooley 2003; Gallo et al. 2006] and very tentative in the case of neutron star XRBs (NSXRBS) [Migliari et al. 2003; Migliari & Fender 2006; Tudose et al. 2009]. A similar behaviour is observed as well in Cyg X-3, as can be seen in Fig. 4 of Szostek et al. (2008) and Fig. 5 of the present work. Unfortunately, this does not offer important hints with respect to the nature of the compact object in the system.

Looking forward to the future, an increase in the number of high resolution observations should offer more insights into the complex behaviour of Cyg X-3. But the quantity of observations in itself is not a guarantee of advancement. Ideally one would have to probe the system in different stages of its evolution. This is certainly doable. Our VLBI detection of the system in a relatively deep quenched state (2008 Apr 9) shows that Cyg X-3 can be traced over a very broad range of flux densities. So far the VLBI observations have been performed almost exclusively in response to major outbursts and if they happen to catch Cyg X-3 in a different state it was mainly due to the slow reaction time of the radio facilities after the triggering. With proper planning, it is possible to trigger on the pre-flare quenched state to observe a major flare at high resolution right from the onset to the end. The e-VLBI technique, with its rapid turnaround

time would then allow to optimize the response to such an outburst by modifying the observing strategy in real time as necessary to best track the development of the flare. Furthermore, it can offer the practical possibility to observe more ephemeral states (like perhaps the post-flare) in which the system spends only days to weeks.

4 CONCLUSIONS

We have reported new e-VLBI radio observations of Cyg X-3 and analyzed them together with previous e-EVN and archival VLBA data. Support MERLIN observations were also presented. We have complemented the radio observations with quasi-simultaneous X-ray data: ASM-RXTE, and in a few cases pointed PCA/HEXTE-RXTE.

It was found that the behaviour of Cyg X-3 at mas scales, as probed here, is well described by the radio/X-ray classification scheme proposed by Szostek et al. (2008) based on arcsec scale radio observations, when the whole contribution of the system to the radio flux density is taken into account (i.e. radio emission from both jet and core). More precisely, this means that our results are in good agreement with those obtained by Szostek et al. (2008) from the point of view of the evolutionary track followed by the system in the radio flux density/X-ray count rate plane as well as from the point of view of the overall normalization of this pathway. Equally important, we didn't find any clear evidence for departures in the behaviour of Cyg X-3 from that expected within the above mentioned model. Some minor question marks were indeed raised by a few observations, but given the small data set available no confident conclusion can be inferred with respect to their origin, statistic or not.

However, when the contribution of the jet to the total radio flux density is removed, and therefore only the radio emission corresponding to the core is considered, the situation changes significantly. What is obvious is that when Cyg X-3 is in an active state (for sure during the major flaring and most of the post-flaring states) the observed radio flux density at cm wavelengths is dominated by the emission from the jet. Hence the data imply that during these states there is no unambiguous connection between the accretion state and the total radio emission.

The mas behaviour of Cyg X-3 during major outbursts seems consistent with the shock-in-jet model (Lindfors et al. 2007; Miller-Jones et al. 2009a) but the interaction of the jet with the surrounding medium should also play a role although its importance is not known for the moment. Hence the more intimate relation between the radio emission of the core and the jet with respect to the radio/X-ray states of the system is not evident from the observations analyzed here. At least partially this is due to the limited size of our data set: only on a few epochs a jet component was present and its contribution to the radio flux quantified. Then the systematic errors associated to the identification of the location of the core might play an important role in altering any such relation. But the prospects for future are not at all bleak. We have shown that the VLBI technique can be a powerful tool in probing the behaviour of Cyg X-3. Carefully chosen observational set-ups (particularly with respect to the selection of the phase referencing calibrator) and, importantly, a

better knowledge of the proper motion of the system, will no doubt alleviate some of the difficulties we encountered in the present analysis.

ACKNOWLEDGMENTS

The European VLBI Network (EVN) is a joint facility of European, Chinese, South African and other radio astronomy institutes funded by their national research councils. e-VLBI developments in Europe are supported by the EC DG-INFOS funded Communication Network Developments project “EXPreS”, Contract No. 02662. The National Radio Astronomy Observatory (NRAO) is a facility of the National Science Foundation operated under cooperative agreement by Associated Universities, Inc. The X-ray data were provided by the ASM/RXTE teams at MIT and at the RXTE SOF and GOF at NASA’s GSFC. AS is supported by the European Community via contract ERC-StG-200911.

REFERENCES

- Arnaud K.A., 1996, in ASP Conf. Ser. 101, *Astronomical Data Analysis Software and Systems V*, eds. G.H. Jacoby and J. Barnes, p. 17
- Becklin E.E., Neugebauer O., Hawkins F., Mason K., Sanford P.W., Matthews K., Wynn-Williams C.G., 1973, *Nature*, 245, 302
- Carpano S., Pollock A.M.T., Prestwich A., Crowther P., Wilms J., Yungelson L., Ehle M., 2007 *A&A*, 466, L17
- Cherepashchuk A.M., Moffat A.F.J., 1994, *ApJ*, 424, L53
- Choudhury M., Rao A.R., Vadawale S.V., Ishwara-Chandra C.H., Jain A.K., 2002, *A&A*, 383, L35
- Coppi P.S., 1992, *MNRAS*, 258, 657
- Coppi P.S., 1999, in ASP Conf. Ser. 161, *High Energy Processes in Accreting Black Holes*, eds. J. Poutanen and R. Svensson, p. 375
- Corbel S., Nowak M.A., Fender R.P., Tzioumis A.K., Markoff S., 2003, *A&A*, 400, 1007
- Corbel S., K rding E., Kaaret P., 2008, *MNRAS*, 389, 1697
- Done C., Gierliński M., Kubota A., 2007, *A&A Rev*, 15, 1
- Fender R.P., Bell Burnell S.J., Waltman E.B., Pooley G.G., Ghigo F.D., Foster R.S., 1997, *MNRAS*, 288, 849
- Fender R.P., Hanson M.M., Pooley G.G., 1999, *MNRAS*, 308, 473
- Gallo E., Fender R.P., Pooley G.G., 2003, *MNRAS*, 344, 60
- Gallo E., Fender R.P., Miller-Jones J.C.A., Merloni A., Jonker P.G., Heinz S., Maccarone T.J., van der Klis M., 2006, *MNRAS*, 370, 1351
- Geldzahler B.J., Johnston K.J., Spencer J.H., Klepczynski W.J., Josties F.J., Angerhofer P.E., Florkowski D.R., McCarthy D.D., Matsakis D.N., Hjellming R.M., 1983, *ApJ*, 273, L65
- Giacconi R., Gorenstein P., Gursky H., Waters J.R., 1967, *ApJ*, 148, L119
- Gierliński M., Zdziarski A.A., Poutanen J., Coppi P.S., Ebisawa K., Johnson W.N., 1999, *MNRAS*, 309, 496
- Greisen E.W., 2003, in *Astrophysics and Space Science Library*, Vol. 285, *Information Handling in Astronomy - Historical Vistas*, ed. A. Heck, p. 109
- Hjalmarsdotter L., Zdziarski A.A., Larsson S., Beckmann V., McCollough M., Hannikainen D.C., Vilhu O., 2008, *MNRAS*, 384, 278
- Hjalmarsdotter L., Zdziarski A.A., Szostek A., Hannikainen D.C., 2009, *MNRAS*, 392, 251
- Koch-Miramond L.,  brah m P., Fuchs Y., Bonnet-Bidaud J.-M., Claret A., 2002, *A&A*, 396, 877
- Lindfors E.J., T rl r M., Hannikainen D.C., Pooley G.G., Tammi J., Trushkin S.A., Valtaoja E., 2007, *A&A*, 473, 923
- Ling Z., Zhang S.N., Tang S., 2009, *ApJ*, 695, 1111
- Magdziarz P., Zdziarski A.A., 1995, *MNRAS*, 273, 837
- Marscher A.P., Gear W.K., 1985, *ApJ*, 298, 114
- Mart  J., Paredes J.M., Peracaula M., 2001, *A&A*, 375, 476
- McCollough M.L., Robinson C.R., Zhang S.N., Harmon B.A., Hjellming R.M., Waltman E.B., Foster R.S., Ghigo F.D., Briggs M.S., Pendleton G.N., Johnston K.J., 1999, *ApJ*, 517, 951
- Migliari S., Fender R.P., Rupen M., Jonker P.G., Klein-Wolt M., Hjellming R.M., van der Klis M., 2003, *MNRAS*, 342, L67
- Migliari S., Fender R.P., 2006, *MNRAS*, 366, 79
- Miller-Jones J.C.A., Blundell K.M., Rupen M.P., Mioduszewski A.J., Duffy P., Beasley A.J., 2004, *ApJ*, 600, 368
- Miller-Jones J.C.A., Rupen M.P., T rl r M., Lindfors E.J., Blundell K.M., Pooley G.G., 2009a, *MNRAS*, 394, 309
- Miller-Jones J.C.A., Sakari C.M., Dhawan V., Tudose V., Fender R.P., Paragi Z., Garrett M., 2009b, in *Proceedings of the 8th International e-VLBI Workshop*, Madrid, Spain, eds. J.E. Conway et al., PoS(EXPreS09)017
- Mioduszewski A.J., Rupen M.P., Hjellming R.M., Pooley G.G., Waltman E.B., 2001, *ApJ*, 553, 766
- Mitra A., 1998, *ApJ*, 499, 385
- Molnar L.A., Reid M.J., Grindlay J.E., 1988, *ApJ*, 331, 494
- Parsignault D.R., Gursky H., Kellogg E.M., Matilsky T., Murray S.S., Schreier E., Tananbaum H., Giacconi R., Brinkman B., 1972, *Nature Phys. Sci.*, 239, 123
- Perley R.A., Schwab F.R., Bridle A.H., 1986, *Course Notes from NRAO Summer School*, Socorro, USA, eds. R.A. Perley, F.R. Schwab and A.H. Bridle
- Predehl P., Burwitz V., Paerels F., Tr mper J., 2000, *A&A*, 357, L25
- Prestwich A.H., Kilgard R., Crowther P.A., Carpano S., Pollock A.M.T., Zezas A., Saar S.H., Roberts T.P., Ward M.J., 2007, *ApJ*, 669, L21
- Pooley G.G., 2006, in *Proceedings of the 6th Microquasar Workshop*, Como, Italy, ed. T. Belloni, PoS(MQW6)019
- Remillard R.A., McClintock J.E., 2006, *ARA&A*, 44, 49
- Rushton A., Spencer R.E., Strong M., Campbell R.M., Casey S., Fender R.P., Garrett M.A., Miller-Jones J.C.A., Pooley G.G., Reynolds C., Szomoru A., Tudose V., Paragi Z., 2007, *MNRAS*, 374, L47
- Schalinski C.J., Johnston K.J., Witzel A., Spencer R.E., Fiedler R., Waltman E., Pooley G.G., Hjellming R., Molnar L.A., 1995, *ApJ*, 447, 752
- Schalinski C.J., Johnston K.J., Witzel A., Waltman E.B., Umana G., Pavelin P.E., Ghigo F.D., Venturi T., Mantovani F., Foley A.R., Spencer R.E., Davis R.J., 1998, *A&A*, 329, 504
- Schmutz W., Geballe T.R., Schild H., 1996, *A&A*, 311, L25
- Shepherd M.C., 1997, in ASP Conf. Ser. 125, *Astronomical*

- Data Analysis Software and Systems VI, eds. G. Hunt and H.E. Payne, p. 77
- Spencer R.E., Swinney R.W., Johnston K.J., Hjellming R.M., 1986, *ApJ*, 309, 694
- Stark M.J., Saia M., 2003, *ApJ*, 587, L101
- Szostek A., Zdziarski A.A., 2008, *MNRAS*, 386, 593
- Szostek A., Zdziarski A.A., McCollough M.L., 2008, *MNRAS*, 388, 1001
- Tavani M., Ruderman M., Shaham J., 1989, *ApJ*, 342, L31
- Trushkin S., Bursov N.N., Nizhelskij N.A., Majorova E.K., Voitsik P.A., 2006, in *Proceedings of the 6th Microquasar Workshop*, Como, Italy, ed. T. Belloni, *PoS(MQW6)015*, preprint [arXiv:astro-ph/0611550](https://arxiv.org/abs/astro-ph/0611550)
- Trushkin S.A., Bursov N.N., Nizhelskij N.A., 2007, *ATel*, 1092, 1
- Trushkin S.A., Nizhelskij N.A., Bursov N.N., 2008, in *Proceedings of the 7th Microquasar Workshop*, Foca, Turkey, ed. E. Kalemci, *PoS(MQW7)032*, preprint [arXiv:0810.3376](https://arxiv.org/abs/0810.3376)
- Tudose V., Fender R.P., Garrett M.A., Miller-Jones J.C.A., Paragi Z., Spencer R.E., Pooley G.G., van der Klis M., Szomoru A., 2007, *MNRAS*, 375, L11
- Tudose V., Paragi Z., Fender R.P., Spencer R.E., Garrett M.A., Rushton A., 2008, *ATel* 1476, 1
- Tudose V., Fender R.P., Linares M., Maitra D., van der Klis M., 2009, accepted to *MNRAS*, [arXiv:0908.3604](https://arxiv.org/abs/0908.3604)
- Türler M., Courvoisier T.J.-L., Paltani S., 2000, *A&A*, 361, 850
- van Kerkwijk M.H., Geballe T.R., King D.L., van der Klis M., van Paradijs J., 1996, *A&A*, 314, 521
- Vilhu O., Hjalmarsdotter L., Zdziarski A.A., Paizis A., McCollough M.L., Beckmann V., Courvoisier T.J.-L., Ebisawa K., Goldoni P., Hakala P., Hannikainen D., Kretschmar P., Westergaard N.J., 2003, *A&A*, 411, L405
- Waltman E.B., Fiedler R.L., Johnston K.L., Ghigo F.D., 1994, *AJ*, 108, 179
- Waltman E.B., Ghigo F.D., Johnston K.J., Foster R.S., Fiedler R.L., Spencer J.H., 1995, *AJ*, 110, 290
- Waltman E.B., Foster R.S., Pooley G.G., Fender R.P., Ghigo F.D., 1996, *AJ*, 112, 2690
- Watanabe H., Kitamoto S., Miyamoto S., Fielder R.L., Waltman E.B., Johnston K.J., Ghigo F.D., 1994, *ApJ*, 433, 350
- Wilkinson P.N., Narayan R., Spencer R.E., 1994, *MNRAS*, 269, 67
- Zdziarski A.A., Gierliński M., 2004, *Prog. Theor. Phys. Suppl.*, 155, 99